Controlling the Orientation, Edge Geometry, and Thickness of Chemical Vapor Deposition Graphene

Adrian T. Murdock,[†] Antal Koos,[†] T. Ben Britton,[†] Lothar Houben,[‡] Tim Batten,[§] Tong Zhang,[§] Angus J. Wilkinson,[†] Rafal E. Dunin-Borkowski,[‡] Christina E. Lekka,[⊥] and Nicole Grobert*[,†]

[†]Department of Materials, University of Oxford, Oxford OX1 3PH, United Kingdom, [‡]Ernst Ruska Centre for Microscopy and Spectroscopy with Electrons, Forschungszentrum Juelich GmbH, 52425 Juelich, Germany, [§]Renishaw plc, Old Town, Wotton-under-Edge, Gloucestershire, GL12 7DW, United Kingdom, and [⊥]Department of Materials Science and Engineering, University of Ioannina, 45110 Ioannina, Greece

ABSTRACT We report that the shape, orientation, edge geometry, and thickness of chemical vapor deposition graphene domains can be controlled by the crystallographic orientations of Cu substrates. Under low-pressure conditions, single-layer graphene domains align with zigzag edges parallel to a single ⟨101⟩ direction on Cu(111) and Cu(101), while bilayer domains align to two directions on Cu(001). Under atmospheric pressure conditions, hexagonal domains also preferentially align. This discovery can be exploited to generate high-quality, tailored graphene with controlled domain thickness, orientations, edge geometries, and grain boundaries.

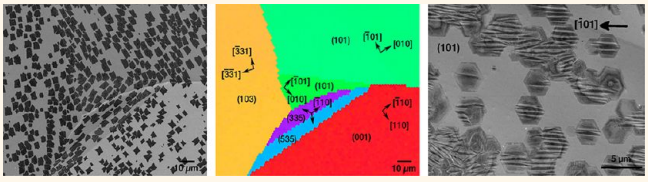

KEYWORDS: graphene · CVD · Cu · orientation · crystallography · EBSD

The industrial exploitation of chemical vapor deposition (CVD) graphene crucially depends on the ability to generate large-area sheets[1,2] with selected thicknesses, predefined domain orientations, edge geometries, and grain boundaries which govern the electronic structure,[3−6] chemical activity,[7] and mechanical strength.[8,9] Unfortunately, precise control of CVD graphene remains unsolved despite tremendous efforts worldwide.[7] The growth of large-area CVD graphene on Cu has developed considerably since it was first demonstrated in 2009.[1] Many researchers have used polycrystalline CVD graphene for device applications.[2,10,11] However, the influence of constituent graphene domains' edge geometries, orientations, and grain boundaries on film quality and device performance has often been overlooked. The CVD growth mechanism has been investigated[12−16] with the aim of consistently producing uniform, high-quality graphene. Synthesis conditions, for example, the pressure, substrate quality, and precursor concentrations, strongly dictate the growth mechanism of graphene domains. Hexagonally shaped domains with defined zigzag edges were synthesized using atmospheric-pressure CVD (APCVD) on Cu foils.[4,17,18] These domains were randomly orientated on the substrate, with misorientation between neighboring domains introducing detrimental structural defects at boundaries.[5,6] Low-pressure CVD (LPCVD) on Cu foils typically produces domains with dendritic features,[14,19,20] although growth with toluene displayed rectangular shapes.[21] LPCVD on evaporated Cu(111) films has also produced high-quality graphene.[22] Low-energy electron microscopy and periodic Moiré patterns revealed that graphene forms epitaxially on single crystalline Cu,[13,16,23,24] but individual domain orientations, edge geometries, and grain boundaries were not investigated. Recently, aligned hexagonal domains were demonstrated using liquid Cu,[25,26] but the orientation relationship between graphene domains and the many different grains that compose a Cu foil (*e.g.*, Cu(001), Cu(111), Cu(101), and high index surface orientations) remains unclear. Indeed, under particular synthesis conditions, researchers have claimed that no epitaxial relationship exists because graphene domains misorient within one Cu grain and show invariant orientation across Cu grain boundaries.[4,20] The ability to control the thickness and orientation of individual

* Address correspondence to nicole.grobert@materials.ox.ac.uk.

Received for review October 23, 2012 and accepted January 24, 2013.

Published online January 24, 2013
10.1021/nn3049297

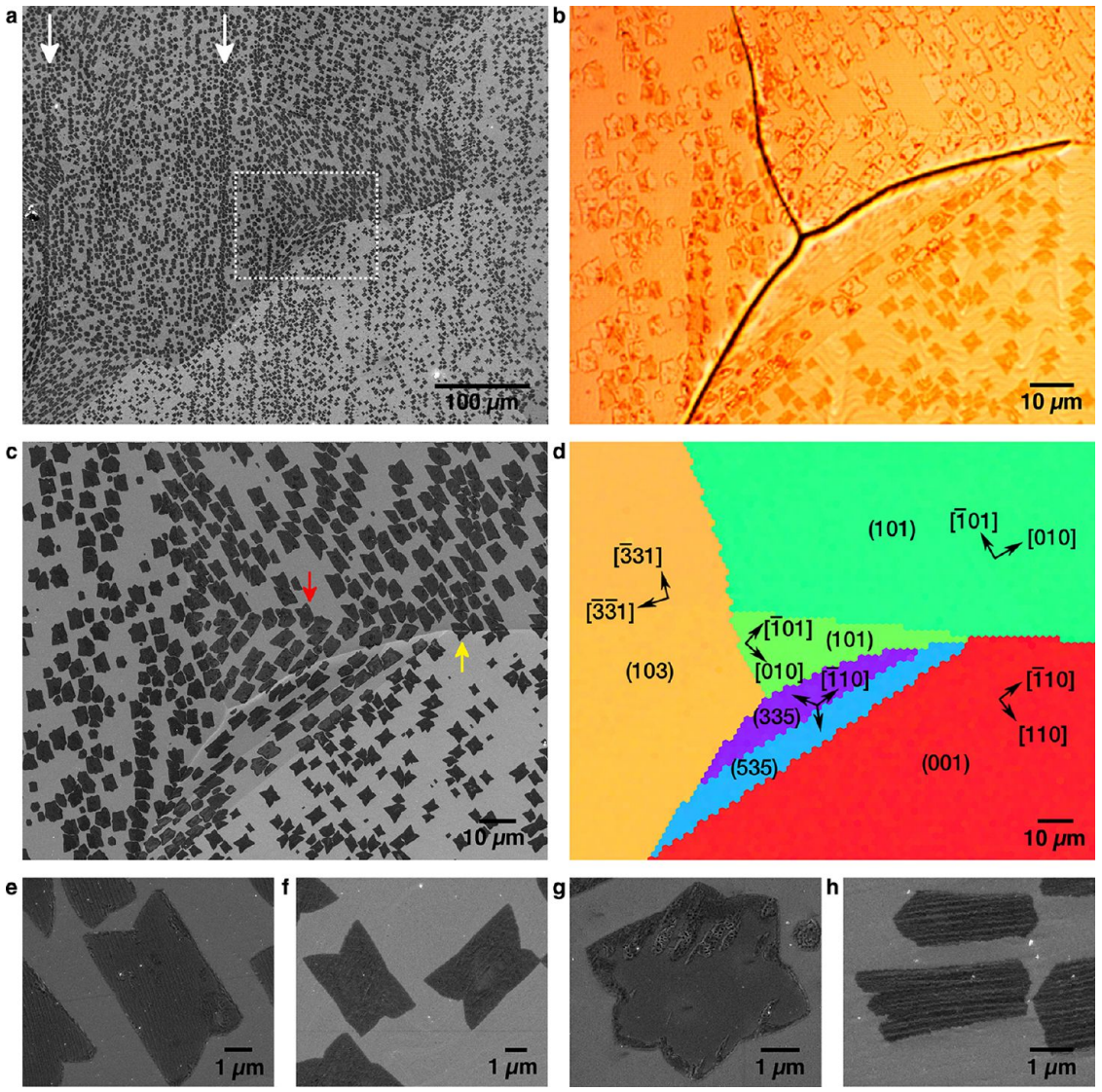

Figure 1. Shape and orientation dependence of LPCVD graphene domains on polycrystalline Cu. a. Low-magnification SEM image demonstrating uniform growth of LPCVD graphene domains on high-purity (99.999%) Alfa Aesar polycrystalline Cu foil. Variations in domain growth on different Cu grains is discernible even at low magnification, while increased nucleation along cold rolling striations is visible (indicated by white arrows). The white box indicates region depicted in b–d. b. Optical micrograph of graphene domains on Cu foil clearly revealing a triple point and twin at the center of the image. Graphene domains formed across grain boundaries and surface terraces. c. SEM image of the same region highlighting variation of LPCVD graphene domain shape and orientation on different Cu grains. A graphene domain spanning across two Cu orientations, Cu{001} and Cu{101}, and changing shape is indicated by the yellow arrow, while the red arrow indicates a domain changing edge orientation across two misoriented grains sharing the same surface normal, Cu{101}. d. Surface normal-projected inverse pole figure EBSD map of the same region of polycrystalline Cu using the standard EBSD color key. Miller indices list the closest low-index crystallographic orientation of each grain, while detailed maps with overlaid unit cubes are provided in Supporting Information Figures S2–S4. Vectors indicate the in-plane orientation of unit cells. Unlabeled vectors on Cu(335) represent component of ⟨101⟩ within the tilted plane, [50–3] and [0–53]. e,f,g,h. SEM images of representative LPCVD graphene domain shapes grown on Cu{101}, Cu{001}, Cu{103}, and orientations close to Cu{111}, *e.g.*, Cu{769}, respectively. See also Supporting Information Figures S1–S7 for SEM, optical microscopy, and EBSD characterization of additional regions.

graphene domains was identified as a key challenge that needs to be addressed for CVD graphene to be used in future applications.[27]

In this article, we report that the crystallographic orientations of polycrystalline Cu substrates can strongly influence the formation of CVD graphene. Our investigations demonstrate a direct link between the atomic-scale orientation and edge geometry of the graphene lattice on Cu surfaces and the macroscopic growth and alignment of graphene domains. This discovery opens a new avenue toward the controlled alignment of individual graphene domains for producing high-quality large-area graphene for integration in transparent conducting electrodes, sensors, and nanoelectronic device applications.[2,28–30]

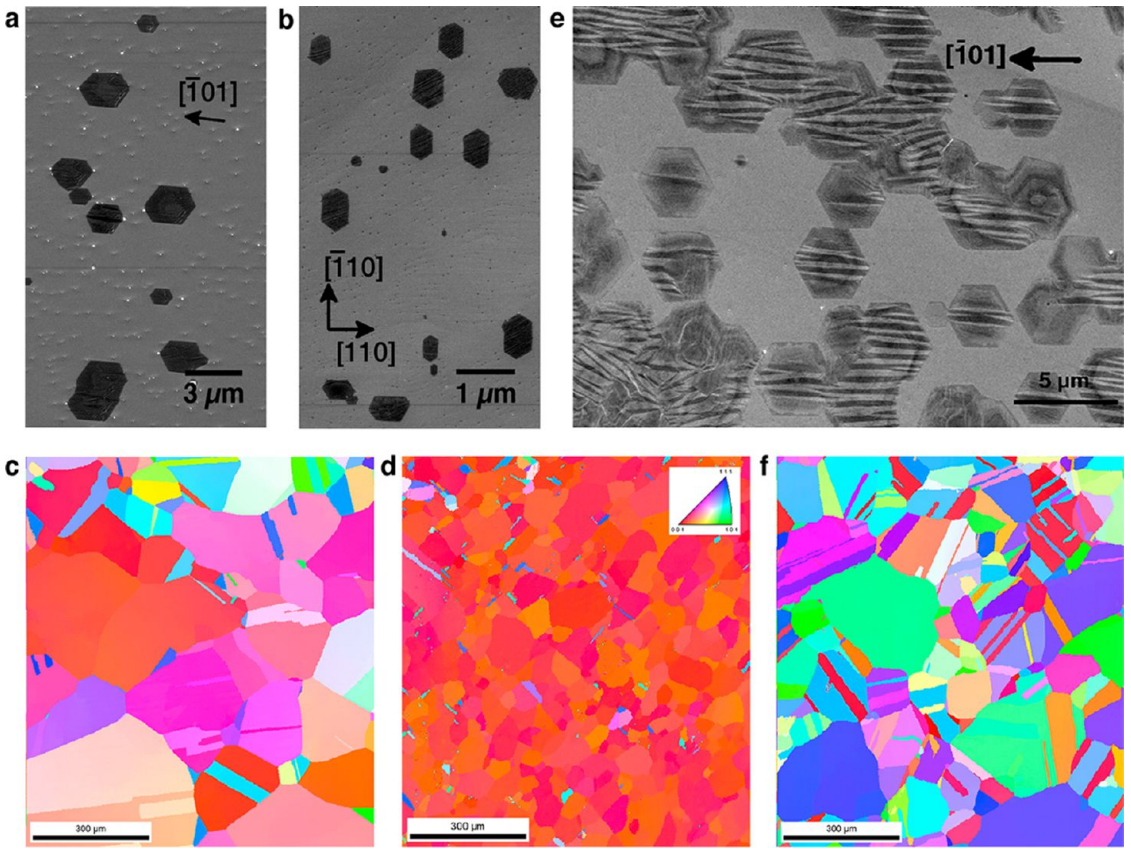

Figure 2. Orientation dependence of APCVD hexagonal graphene domains on polycrystalline Cu. a,b. SEM images of APCVD hexagonal graphene domains grown on high purity (99.999%) Alfa Aesar Cu foil, demonstrating alignment to one direction on Cu{111} and two directions on Cu{001}, respectively. c,d. Low magnification, 1000 × 900 μm, surface normal-projected inverse pole figure EBSD maps of high-purity (99.999%) and low-purity (99.8%) Alfa Aesar Cu foil, respectively, with color key inset. e. SEM image of APCVD hexagonal graphene domains grown on low-purity (99.9%) Goodfellow Cu foil, demonstrating alignment to one direction on Cu{101}. f. Low magnification, 1000 × 900 μm, surface normal-projected inverse pole figure EBSD map of low-purity (99.9%) Goodfellow Cu foil, demonstrating prevalence of grains with orientation near Cu{101} and Cu{111}.

RESULTS AND DISCUSSION

Distinctive shapes of single crystal graphene domains with specific orientations were synthesized using LPCVD and APCVD in conjunction with high relative hydrogen pressures on high-purity Cu substrates (99.999%, Alfa Aesar). Following LPCVD, isolated graphene domains grew uniformly across substrates (>2 cm^2) (Figure 1a,b) owing to a purposely selected short synthesis time (1 min) to avoid significant domain coalescence. Domain growth continued across large-scale topographical features, *e.g.* cold-rolling striations, Cu grain boundaries, and surface terraces, though some influence on domain alignment, shape, and nucleation density was observed. Distinct shapes and orientations of LPCVD graphene domains were identified on different regions of the substrate with variations corresponding to different Cu grains and grain boundaries.

We used scanning electron microscopy (SEM) (Figure 1c) and electron backscatter diffraction (EBSD) mapping (Figure 1d) to correlate the different LPCVD graphene domain shapes and their orientations with the crystallographic orientation of the respective Cu grains and identified four predominant cases:

- *Four-lobed, parallel-sided domains* (Figure 1e) on Cu(101) (green), orientated in one direction, *i.e.,* [−101].
- *Four-lobed, parallel-sided domains* (Figure 1f) on Cu(001) (red), orientated in two ∼90° rotated directions with equal probability, *i.e.,* near [110] and [−110].
- *Six-lobed, star-shaped domains* (Figure 1g) on tilted and high-index Cu grains, *e.g.*, Cu(103) (orange), with only minor alignment, *i.e.*, [−331].
- *Hexagonal-edged elongated domains* (Figure 1h) on orientations close to Cu(111), *e.g.*, Cu(335) (purple) and Cu(535) (blue), orientated in one direction, *i.e.*, [−110]. Hexagonal edges align to components of [10−1] and [0−11] in the plane of the tilted surface, *i.e.*, [50−3] and [0−53] for Cu(335).

While the four-lobed domains on Cu(101) and Cu(001) show similarities to those previously reported,[14,15] the parallel edges and alignment suggest that additional

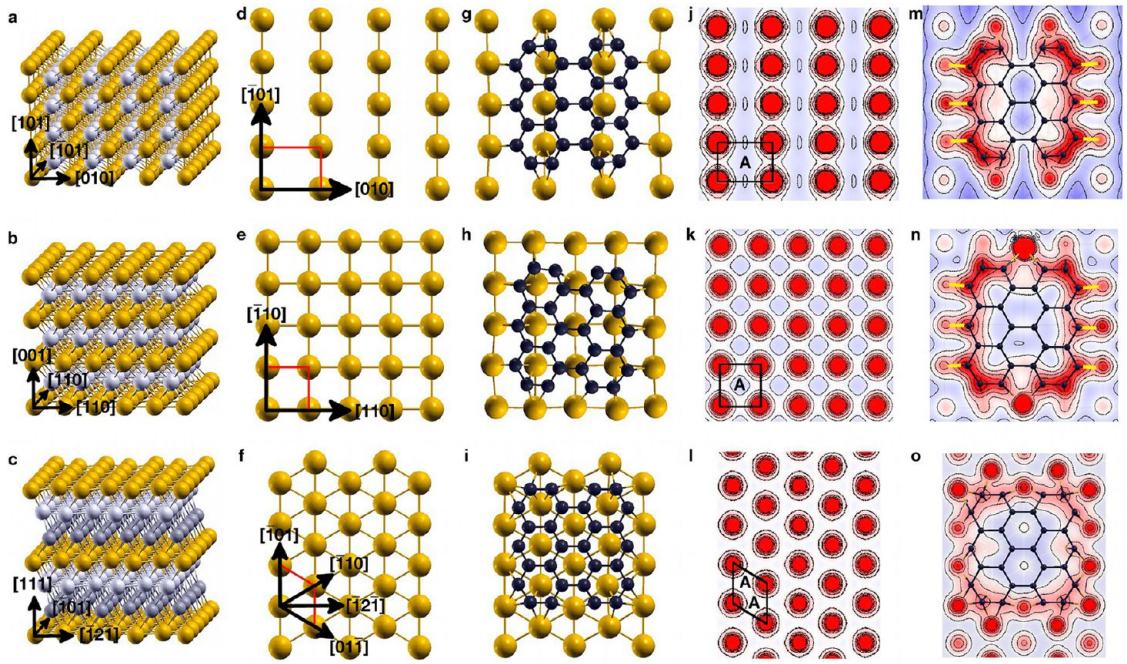

Figure 3. Computational modeling of graphene clusters on Cu{101}, Cu{001}, and Cu{111}. a,b,c. Three-dimensional side-on view of the crystal structure of Cu(101), Cu(001), and Cu(111), respectively, with surface normal pointing upward as indicated by vectors. Different colored spheres represent the second (third) atomic layers. Cu(101) is the most open surface displaying the conspicuous channels that promote deposition and surface diffusion in [−101] direction.[32] d. Cu(101) 2-fold symmetrical rectangular lattice with unit cell $a = 3.615$ Å and $a(\sqrt{2}/2) = 2.556$ Å. e. Cu(001) 4-fold symmetrical square lattice with unit cell $a(\sqrt{2}/2) = 2.556$ Å. f. Cu(111) 6-fold symmetrical hexagonal lattice with unit cell $a(\sqrt{2}/2) = 2.556$ Å. g,h,i. Model graphene domain, C_{28}, on Cu(101), Cu(001), and Cu(111), respectively, demonstrating preferential edge orientation with Cu ⟨101⟩ direction(s), taking into account the graphene zigzag edge ($a_{cc}\sqrt{3} = 2.46$ Å) and armchair edge ($3a_{cc} = 4.26$ Å). j,k,l. Total electron density plot of Cu{101}, Cu{001}, and Cu{111}, respectively. Red circles correspond to the surface atoms (high electron density), while regions with depleted electron density are equivalent to available adatom sites (labeled A). m,n,o. Total electron density contour plot for graphene cluster, C_{28}, on Cu(101), Cu(001), and Cu(111), respectively, projected at the interlayer plane between the substrate and C_{28}. Electron density increases from blue to red. Strong one-to-one hybridization occurs along the Cu ⟨101⟩ direction between the electron orbitals of the zigzag edge atoms of C_{28} and Cu surface atoms on Cu(101) and Cu(001), indicated by yellow lines. Weaker one-to-two atom bonding between one C and two Cu atoms is observed on Cu(111).

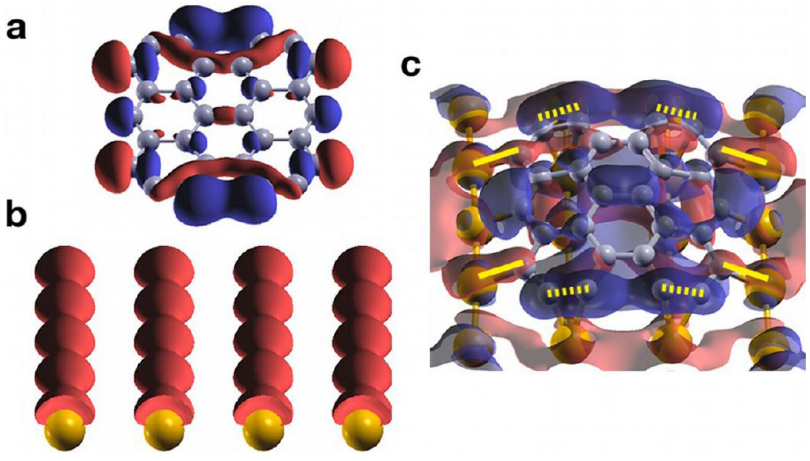

Figure 4. Wave function representation of graphene cluster on Cu{101}. a. Wave function at the Fermi level for free-standing C_{28} graphene cluster, showing the 2p C orbitals along the zigzag edges. b. Wave function at the Fermi level for Cu{101} surface layer. Lobes of the 3d electrons point outward, while characteristic channels show electron depletion. c. Wave function at the Fermi level for C_{28} graphene cluster on Cu{101}. Blue and red regions correspond to the positive and negative values of the wave function, respectively. On the zigzag edge of C_{28}, the red lobes of the 2p C orbitals hybridize with red lobes of the 3d Cu orbitals to form directional bonds (solid yellow lines), while blue lobes represent active sites. On the armchair edge of C_{28}, hybridization occurs between neighboring C atoms (dashed yellow lines).

factors influence domain formation. For orientations close to Cu(111), the presence of terraces and lattice steps influence the growth causing elongation of domains parallel to the step direction, *i.e.*, [−110]. Similarly, terraces on tilted and high-index Cu grains such as Cu(103) cause minor domain alignment as

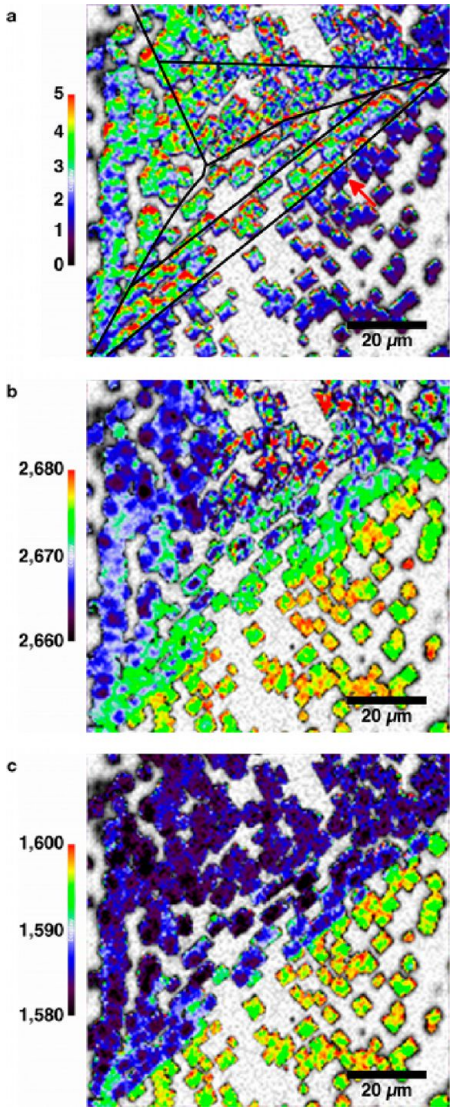

Figure 5. Spatially resolved Raman spectroscopy maps (90 × 90 μm^2) corresponding to the Cu substrate area depicted in Figure 1. a. Map showing variation of 2D and G peak intensity ratio, I_{2D}/I_G, for graphene domains on different Cu grains. Black lines indicate Cu grain boundaries. On Cu{103}, Cu{535}, and Cu{335}, the ratio is $I_{2D}/I_G > 3$ demonstrating single-layer graphene. On Cu{001}, the ratio is $1 < I_{2D}/I_G < 2$ indicating bilayer graphene. On Cu{101}, the ratio varies but is consistently $I_{2D}/I_G > 1$, indicating that both single and bilayer graphene form. A change in I_{2D}/I_G is observed for graphene domains spanning across two Cu orientations, *e.g.*, Cu{001} and Cu{535}, indicated by the red arrow. b,c. 2D and G peak position, respectively, illustrating shifts in the peak position correlating with Cu crystallographic orientation. The peak-shift is a result of substrate-induced strain (see Supporting Information).

multiple factors influence domain growth (see Supporting Information).

SEM and EBSD mapping also demonstrated that when LPCVD graphene domains crossed Cu grain boundaries their shape and orientation changed accordingly because of the different Cu crystallographic orientations. Transitions occurred for domain growth over two different Cu crystallographic orientations, *e.g.*, Cu{001} and Cu{101} (Figure 1c; yellow arrow), and for growth over two misoriented grains sharing the same surface normal, *e.g.*, domains growing across two neighboring Cu(101) grains that possess a relative in-plane misorientation of 68° (Figure 1d; green, and pale green regions) align to the [−101] direction of each grain (Figure 1c, red arrow; Supporting Information Figure S5). The edge orientations of graphene domains are therefore directly related to a specific crystal direction of the Cu surface, and not solely to the crystallographic orientation. Graphene domains therefore grow epitaxially with preferential orientation along the Cu ⟨101⟩ direction.

Characteristic hexagonal-shaped graphene domains were also synthesized *via* APCVD on high-purity Cu substrates (99.999%, Alfa Aesar) and showed edge alignment parallel to ⟨101⟩, in one direction on Cu{101} and Cu{111} (Figure 2a), and in two ∼90° rotated directions on Cu{001} (Figure 2b and Supporting Information Figure S11). This is identical to our observations for LPCVD growth. It is noteworthy that domain alignment was not immediately discernible on Cu{001} due to the 6-fold symmetrical hexagonal domains orientating to the two ⟨101⟩ directions on this surface. We also conducted investigations with commonly used low-purity Cu foils (99.8%, Alfa Aesar) and again observed preferential alignment of the hexagonal graphene domains (see Supporting Information Figure S12). On this substrate, the domains showed an increased misalignment compared to high-purity Cu foils, which we believe is due to greater topographical variations. EBSD mapping demonstrated that the high-purity Alfa Aesar Cu foils contain Cu{101} and Cu{111} (Figure 2c), while the low-purity Alfa Aesar Cu foils are dominated by Cu{001} (Figure 2d) resulting in edge alignment of hexagonal domains to two ∼90° rotated directions. The abundance of Cu{001} on the low-purity Alfa Aesar Cu foils explains why alignment has not been previously identified on this substrate. In comparison, distinctive edge alignment of hexagonal domains is easily identified on low-purity Cu foils purchased from an alternative supplier (99.9%, Goodfellow) (Figure 2e) due to the prevalence of large grains with orientations near Cu{111} and Cu{101} (Figure 2f). Epitaxial growth and edge alignment is therefore observed for a wide range of synthesis pressures and with various purities of Cu foil, with the crucial requirement for alignment of domain edges to one direction being the presence of Cu grains exhibiting crystallographic orientations of Cu{101} or Cu(111}.

The discovery of substrate-controlled edge alignment of hexagonal graphene domains is an important advance toward the development of high-quality, large-area CVD graphene composed of perfectly orientated hexagonal domains that merge together with ideal, low-angle, defect-free grain boundaries. Our studies clarify why, to date, this phenomenon has been

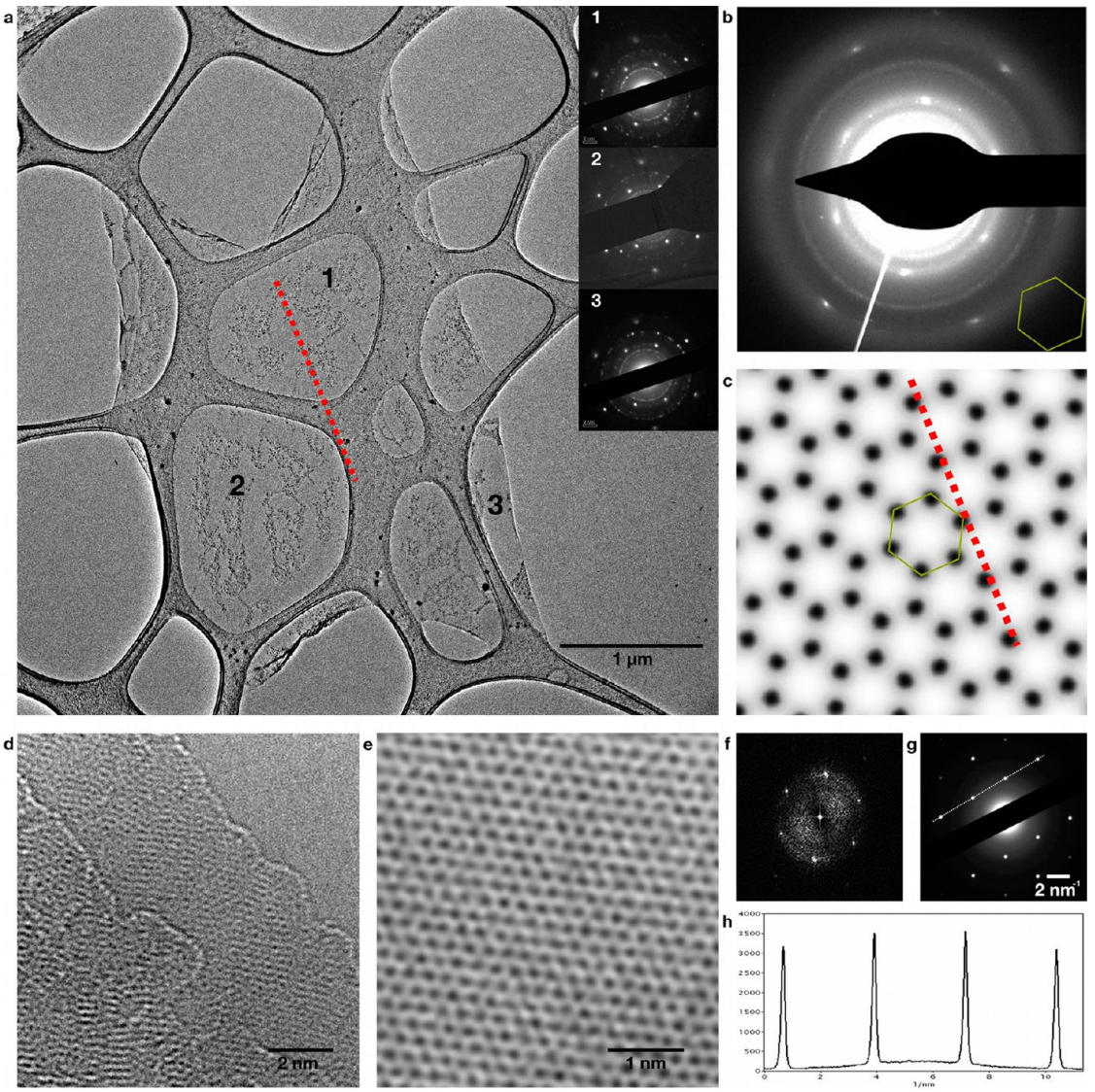

Figure 6. TEM and SAED studies of graphene domain edge geometry and thickness. a. Low-magnification TEM image of a single domain identified as originating from Cu{001} orientation owing to (i) characteristic 4-lobed, parallel-sided shape, and (ii) the domain's proximity to other domains 90° misoriented. The domain was confirmed as single crystalline because of the invariant orientation of SAED patterns taken across the substrate at points 1, 2, and 3 (see insets). Irregular contrast due to PMMA residues is also visible. b. SAED over entire domain elucidates orientation of graphene lattice. c. Orientation of graphene lattice from b, indicating zigzag geometry of the long axis (red dashed line in a and c). d. High-resolution TEM imaging of the domain originating from Cu{001} confirmed bilayer graphene and revealed that the PMMA transfer process damaged the pristine zigzag edge geometry.[4] e,f,g,h. High-resolution imaging, associated FFT, SAED pattern, and associated line profile, respectively, for a different graphene domain originating from Cu{101} or an orientation close to Cu{111}, confirming domain as single-layer graphene.

largely overlooked. We found that epitaxial growth and alignment occurred for LPCVD and APCVD synthesis, for low-purity and high-purity Cu (99.8% and 99.999%), and for Cu foil sourced from two different suppliers (Alfa Aesar and Goodfellow). We therefore conclude that epitaxial growth is directly related to the crystallographic orientation of the Cu substrate, and is independent of the Cu purity and supplier.

As large-area graphene domains are commonly single crystalline, we hypothesize that their alignment can be dictated by a preferential orientation of nanoscale nucleating domains on the Cu surface. Computational modeling provides an opportunity to investigate this, corroborating our experimental observations and providing further insight. We modeled the three low-index orientations, Cu{101}, Cu{001}, and Cu{111}, which exhibit rectangular, square, and hexagonal lattices, respectively (Figures 3a–f), and found that the hexagonal graphene lattice shows varying affinity for the different orientations. Therefore, a decisive factor during domain formation is the minimization of lattice mismatch between graphene and the Cu. Electron hybridization may also stabilize and promote domain growth.

Figure 3g–i show a model graphene cluster (C_{28}) relaxed on each surface demonstrating orientation of zigzag edges with the ⟨101⟩ direction, irrespective of Cu

crystallographic orientation. C hexagons preferentially locate above Cu atoms at available adatom sites, *i.e.*, low electron density sites (Figure 3j–l). Although alternative orientations of C_{28} on anisotropic Cu{101} produced a lattice mismatch (Supporting Information Figure S14), on Cu(001) the C_{28} cluster showed equivalent preference to align with zigzag edges parallel to [110] or [−110] due to the symmetrical lattice (Figure 3e).[16,23,24] This is in agreement with the experimentally observed alignment of graphene domains to one direction on Cu{111} and Cu{101}, and two ∼90° rotated alignments on Cu{001}.

The characteristic zigzag edge dangling bonds of graphene,[31] represented in C_{28}, form directional bonds with Cu surface atoms along the ⟨101⟩ direction(s) on Cu{101} and Cu{001}, thereby stabilizing the cluster (Figure 3m,n), while on Cu{111}, the zigzag edge atoms hybridize with two neighboring Cu atoms (Figure 3o). The outermost armchair edge atoms of C_{28} hybridize mainly among themselves, as reported for graphene armchair edges,[31] and for all surfaces, there is enhanced electron density near the corner of the C_{28} cluster representing potential growth sites in the [−101] direction, *i.e.*, corresponding to experimentally observed lobes in LPCVD domains.

The wave function at the Fermi level (WF) of C_{28} shows characteristic open 2p C orbitals along the zigzag edge (Figure 4a).[31] For Cu(101), with $3d_{eg}$ orbitals of surface atoms pointing outward, the WF demonstrates that the surface channels[32] exhibit electron depletion aligned along the [−101] direction (Figure 4b). When C_{28} is placed on Cu{101}, the zigzag edge atoms alternate between hybridizing with the surface and manifesting active sites, while armchair edge atoms instead hybridize among themselves (Figure 4c).

The presence of the surface channel, emergence of 2p-3d hybridization, and the relatively small lattice mismatch explain the experimentally observed stability and [−101] orientation of graphene domains on Cu(101). For channel-free surfaces, such as Cu{001} and Cu{111}, growth is likely to occur along the zigzag edge, in agreement with calculations for the favorable attachment of monomers to armchair edges.[17] Zigzag edges are therefore promoted on Cu{001} and Cu{111}.

Besides the influence of lattice matching and electron density correlations on the growth of graphene, the role of hydrogen is crucial in the CVD reaction mechanism. Hydrogen may act as a co-catalyst, promoting growth preferentially along the Cu ⟨101⟩ direction(s), or as an etchant, thereby restricting growth to zigzag edges.[18]

Apart from domain orientation, technological applications are crucially dependent on the thickness and edge geometry of graphene materials. Spatially resolved Raman spectroscopy (Figure 5 and Supporting Information Figure S13) revealed that the quality and thickness of LPCVD graphene domains are dictated by Cu crystallographic orientations. Raman peak intensity ratios (I_{2D}/I_G) (Figure 5a) correlate with crystallographic orientations of the Cu substrate (Figure 1d). Since $I_{2D}/I_G > 2$, single-layer graphene preferentially forms on Cu{103} and orientations close to Cu{111}, *i.e.*, Cu{535} and Cu{335}. Bilayer graphene forms on Cu{001} since $1 < I_{2D}/I_G < 2$. These observations agree with results by Wood *et al.*[33] indicating that single and multilayer graphene form on Cu{111} and Cu{001}, respectively. Graphene domains spanning across Cu{535} and Cu{001} show both single and bilayer spectra, dictated by the underlying Cu grain. The crystallographic orientation of the Cu substrate therefore strongly influences the type of LPCVD graphene that forms. We believe that the thickness variations of LPCVD graphene domains on different Cu crystallographic orientations arise from differences in the interaction between the domains and the substrate surface. Nie *et al.*[34] have recently demonstrated that bilayer graphene can form from secondary layers growing underneath an initial domain. Our computational modeling indicates less affinity between the graphene adlayer and Cu{001} compared to other Cu crystallographic orientations, which would increase the likelihood of diffusion of carbon species underneath domains on Cu{001} and the formation of bilayer graphene. Further investigations will be necessary to fully understand and optimize this phenomenon.

The effect of substrate-induced strain in graphene domains is also detected by spatially resolved Raman spectroscopy, as 2D and G peak positions vary with Cu crystallographic orientation (Figure 5b,c; Supporting Information Figure S13).

Edge geometries of LPCVD graphene domains were investigated by correlating transmission electron microscopy (TEM) images (Figure 6a) with the orientation of selected area electron diffraction (SAED) patterns (Figure 6b,c). The long axes of domains were found to be zigzag for all investigated. Consequently, the two parallel edges of the LPCVD graphene domains show zigzag geometry (Figure 6c). While multilobed graphene domains may be composed of several single crystals,[9,15] SAED patterns taken from multiple regions across a domain did not rotate relative to each other, thereby demonstrating single crystal graphene (insets, Figure 6a).

CONCLUSION

We have demonstrated that the shape, orientation, edge geometry, and thickness of CVD graphene domains strongly depend on the crystallographic orientation of polycrystalline Cu substrates. Graphene domains form epitaxially with macroscopic edges orienting parallel to Cu ⟨101⟩ direction(s). LPCVD graphene domain thickness and edge geometry are also dictated by the substrate, with high-quality single-layer graphene forming on orientations close to Cu{111} and bilayer on Cu{001}, while aligned edges exhibit zigzag geometry. APCVD hexagonal graphene domains align with edges parallel to one Cu ⟨101⟩

direction on Cu{111} and Cu{101}, and two directions on Cu{001}. Computational modeling corroborated experimental observations, with domain zigzag edges preferentially aligning parallel to the ⟨101⟩ direction for Cu{001}, Cu{101}, and Cu{111}. Our findings are essential for understanding the optimum parameters for controlling and predefining constituent graphene domains necessary for the production of uniform high-quality, large-area graphene with selected properties.

METHODS

Synthesis of CVD Graphene on Cu Foils. Graphene was synthesized using low-pressure chemical vapor deposition of CH_4 in the presence of H_2 on 10 × 25 mm^2 as-received 25-μm-thick Cu foils (99.999%; Alfa Aesar, item no. 10950). The CVD setup consisted of a quartz tube (20 mm inner-diameter) located inside a horizontal cylindrical furnace and connected to a scroll pump. The Cu substrates were placed inside the quartz tube and kept 10 cm outside the furnace before the system was evacuated to a base pressure of <0.01 Torr, purged with Ar, and backfilled with 500 sccm H_2 at 4.1 Torr. Following this, the furnace was heated to 1035 °C and left until the temperature stabilized before the Cu substrates were rapidly heated by shifting them into the hot zone of the furnace. The Cu substrates were kept at 1035 °C for 30 min in the presence of 500 sccm H_2 to clean the surface, increase the Cu grain size, and promote the formation of preferred crystallographic orientations. Once the substrates were annealed, 5 sccm CH_4 was introduced for 1 min without changing the H_2 flow to grow graphene on the Cu substrate. During the graphene growth, the pressure was 4.2 Torr. After the growth period, the CH_4 was switched off and the substrates were quenched by rapidly shifting out of the hot zone to cool in a H_2 atmosphere. For APCVD, the scroll pump was replaced with an acetone bubbler. Cu substrates were annealed under 500 sccm H_2 for 30 min. Following annealing, the H_2 flow was decreased to 300 and 5 sccm CH_4 was introduced for 15 min. Low-purity Cu foils (99.8%, Alfa Aesar, and 99.9%, Goodfellow) were used for investigations following 10 min sonication in acetic acid and rinsing in deionized water, to remove contaminants from surface coatings applied by suppliers.[21]

Transfer of Graphene Samples. Graphene samples were transferred from Cu to alternative substrates using a poly(methyl methacrylate) (PMMA) supporting film.[1] PMMA (M_w ~996 000) was dissolved in chlorobenzene at 120 °C (20 mg/mL) and drop-coated onto the graphene-covered Cu. PMMA coated substrates were then cured in an oven at 180 °C for 1 min. Samples were floated on ~0.2 g/mL $FeNO_3$ to etch away the Cu, leaving PMMA/graphene samples floating on the surface of the liquid. The etching solution was replaced with deionized water and the PMMA/graphene samples were transferred onto the target substrate, *e.g.*, TEM grid or 300 nm SiO_2/Si. The PMMA was dissolved using warm acetone leaving graphene on the target substrate. Graphene-coated substrates were heated to 180 °C in a vacuum oven for 60 min to aid the removal of residual PMMA from the surface.

Characterization of Samples. Samples were characterized by SEM, EBSD, TEM and SAED, Raman spectroscopy, and optical microscopy. A JEOL JSM-6500F was operated at 5 kV for SEM imaging and 15 kV for EBSD measurements taken with 2 μm step size. TEM and SAED were conducted on a JEOL 2010 TEM operated at 200 kV. The rotation between the TEM images and corresponding SAED patterns was calibrated using molybdenum trioxide crystals. High-resolution TEM was conducted on a Titan G2 60−300 operated at 80 kV. A Renishaw inVia Raman spectrometer equipped with a 532 nm laser and operated in StreamLine Plus mode was used to collect Raman mapping data. Optical microscopy was conducted using a Reichert Polyvar MET optical microscope.

Computational Modeling. We applied the standard Kohn−Sham self-consistent density functional theory (DFT) to local density approximation calculations using the SIESTA code. Core electrons were replaced by norm-conserving pseudopotentials in the fully nonlocal Kleinman-Bylander form and the basis set was a general and flexible linear combination of numerical atomic orbitals constructed from the eigenstates of the atomic pseudopotentials.[35] The nonlocal partial core exchange correlation correction was included for Cu to improve the description of the core valence interactions.[36] An auxiliary real space grid equivalent to a plane-wave cutoff of 100 Ry was used.

Three Cu surfaces were simulated using five-layer (4 × 4), (6 × 4), and (3 × 5) unit cells forming infinite slabs with {001}, {101}, and {111} surface normals, thus resulting in systems having 188, 148, and 178 atoms, respectively. Each system was sampled with four (2 × 2 × 1) in-plane *k*-points and a vacuum of 20 Å. For the graphene sheet, we used a rectangular cluster, C_{28}, consisting of zigzag and armchair edges. In order to verify that the size of the system used and the contribution of edge states does not affect the obtained results, we performed calculations with double the size of graphene adlayer-substrates (C_{54}) and found that the preferential orientation remains unchanged. During the geometry optimizations, all atoms were relaxed, except the last two layers that were kept fixed, thus mimicking the bulk positions. All calculations were performed within the spin-polarized frame.

Conflict of Interest: The authors declare no competing financial interest.

Supporting Information Available: Experimental and theoretical methods, additional OM, SEM, EBSD images, Raman spectroscopy. This material is available free of charge *via* the Internet at http://pubs.acs.org.

Acknowledgment. We are grateful to the Commonwealth Scholarship Commission (A.T.M.), University of Oxford Clarendon Fund (A.T.M.), the Royal Society (N.G.), the European Research Council (ERC-2009-StG-240500) (N.G.), the Engineering and Physical Sciences Research Council Pathways to Impact Awards (N.G.), and EPSRC − EP/H018921/1 (T.B.B.) for financial support.

REFERENCES AND NOTES

1. Li, X.; Cai, W.; An, J.; Kim, S.; Nah, J.; Yang, D.; Piner, R. D.; Velamakanni, A.; Jung, I.; Tutuc, E.; et al. Large-Area Synthesis of High-Quality and Uniform Graphene Films on Copper Foils. *Science* **2009**, *324*, 1312–1314.
2. Bae, S.; Kim, H.; Lee, Y.; Xu, X.; Park, J.-S.; Zheng, Y.; Balakrishnan, J.; Lei, T.; Ri Kim, H.; Song, Y. I.; et al. Roll-to-Roll Production of 30-Inch Graphene Films for Transparent Electrodes. *Nat. Nanotechnol.* **2010**, *5*, 574–578.
3. Yazyev, O. V.; Louie, S. G. Electronic Transport in Polycrystalline Graphene. *Nat. Mater.* **2010**, *9*, 806–809.
4. Yu, Q.; Jauregui, L. A.; Wu, W.; Colby, R.; Tian, J.; Su, Z.; Cao, H.; Liu, Z.; Pandey, D.; Wei, D.; et al. Control and Characterization of Individual Grains and Grain Boundaries in Graphene Grown by Chemical Vapour Deposition. *Nat. Mater.* **2011**, *10*, 443–449.
5. Tapaszto, L.; Nemes-Incze, P.; Dobrik, G.; Yoo, K. J.; Hwang, C.; Biro, L. P. Mapping the Electronic Properties of Individual Graphene Grain Boundaries. *Appl. Phys. Lett.* **2012**, *100*, 053114.
6. Banhart, F.; Kotakoski, J.; Krasheninnikov, A. V. Structural Defects in Graphene. *ACS Nano* **2011**, *5*, 26–41.
7. Sun, Z.; James, D. K.; Tour, J. M. Graphene Chemistry: Synthesis and Manipulation. *J. Phys. Chem. Lett.* **2011**, *2*, 2425–2432.
8. Grantab, R.; Shenoy, V. B.; Ruoff, R. S. Anomalous Strength Characteristics of Tilt Grain Boundaries in Graphene. *Science* **2010**, *330*, 946–948.

9. Huang, P. Y.; Ruiz-Vargas, C. S.; van der Zande, A. M.; Whitney, W. S.; Levendorf, M. P.; Kevek, J. W.; Garg, S.; Alden, J. S.; Hustedt, C. J.; Zhu, Y.; et al. Imaging Grains and Grain Boundaries in Single-Layer Graphene: An Atomic Patchwork Quilt. *Nature* **2011**, *469*, 389–392.
10. Levendorf, M. P.; Ruiz-Vargas, C. S.; Garg, S.; Park, J. Transfer-Free Batch Fabrication of Single Layer Graphene Transistors. *Nano Lett.* **2009**, *9*, 4479–4483.
11. Li, X.; Zhu, Y.; Cai, W.; Borysiak, M.; Han, B.; Chen, D.; Piner, R. D.; Colombo, L.; Ruoff, R. S. Transfer of Large-Area Graphene Films for High-Performance Transparent Conductive Electrodes. *Nano Lett.* **2009**, *9*, 4359–4363.
12. Bhaviripudi, S.; Jia, X.; Dresselhaus, M. S.; Kong, J. Role of Kinetic Factors in Chemical Vapor Deposition Synthesis of Uniform Large Area Graphene Using Copper Catalyst. *Nano Lett.* **2010**, *10*, 4128–4133.
13. Gao, L.; Guest, J. R.; Guisinger, N. P. Epitaxial Graphene on Cu(111). *Nano Lett.* **2010**, *10*, 3512–3516.
14. Li, X.; Magnuson, C. W.; Venugopal, A.; An, J.; Suk, J. W.; Han, B.; Borysiak, M.; Cai, W.; Velamakanni, A.; Zhu, Y.; et al. Graphene Films With Large Domain Size by a Two-Step Chemical Vapor Deposition Process. *Nano Lett.* **2010**, *10*, 4328–4334.
15. Wofford, J. M.; Nie, S.; McCarty, K. F.; Bartelt, N. C.; Dubon, O. D. Graphene Islands on Cu Foils: the Interplay Between Shape, Orientation, and Defects. *Nano Lett.* **2010**, *10*, 4890–4896.
16. Zhao, L.; Rim, K. T.; Zhou, H.; He, R.; Heinz, T. F.; Pinczuk, A.; Flynn, G. W.; Pasupathy, A. N. Influence of Copper Crystal Surface on the CVD Growth of Large Area Monolayer Graphene. *Solid State Commun.* **2011**, *151*, 509–513.
17. Luo, Z.; Kim, S.; Kawamoto, N.; Rappe, A. M.; Johnson, A. T. C. Growth Mechanism of Hexagonal-Shape Graphene Flakes with Zigzag Edges. *ACS Nano* **2011**, *5*, 9154–60.
18. Vlassiouk, I.; Regmi, M.; Fulvio, P.; Dai, S.; Datskos, P.; Eres, G.; Smirnov, S. Role of Hydrogen in Chemical Vapor Deposition Growth of Large Single-Crystal Graphene. *ACS Nano* **2011**, *5*, 6069–76.
19. Li, X.; Magnuson, C. W.; Venugopal, A.; Tromp, R. M.; Hannon, J. B.; Vogel, E. M.; Colombo, L.; Ruoff, R. S. Large-Area Graphene Single Crystals Grown by Low-Pressure Chemical Vapor Deposition of Methane on Copper. *J. Am. Chem. Soc.* **2011**, *133*, 2816–2819.
20. Zhang, Y.; Zhang, L.; Kim, P.; Ge, M.; Li, Z.; Zhou, C. Vapor Trapping Growth of Single-Crystalline Graphene Flowers: Synthesis, Morphology, and Electronic Properties. *Nano Lett* **2012**, *12*, 2810–2816.
21. Zhang, B.; Lee, W. H.; Piner, R.; Kholmanov, I.; Wu, Y.; Li, H.; Ji, H.; Ruoff, R. S. Low-Temperature Chemical Vapor Deposition Growth of Graphene From Toluene on Electropolished Copper Foils. *ACS Nano* **2012**, *6*, 2471–2476.
22. Tao, L.; Lee, J.; Chou, H.; Holt, M.; Ruoff, R. S.; Akinwande, D. Synthesis of High Quality Monolayer Graphene at Reduced Temperature on Hydrogen Enriched Evaporated Copper (111) Films. *ACS Nano* **2012**, *6*, 2319–2325.
23. Rasool, H. I.; Song, E. B.; Mecklenburg, M.; Regan, B. C.; Wang, K. L.; Weiller, B. H.; Gimzewski, J. K. Atomic-Scale Characterization of Graphene Grown on Copper (100) Single Crystals. *J. Am. Chem. Soc.* **2011**, *133*, 12536–43.
24. Ogawa, Y.; Hu, B.; Orofeo, C. M.; Tsuji, M.; Ikeda, K.; Mizuno, S.; Hibino, H.; Ago, H. Domain Structure and Boundary in Single-Layer Graphene Grown on Cu(111) and Cu(100) Films. *J. Phys. Chem. Lett.* **2012**, *3*, 219–226.
25. Geng, D.; Wu, B.; Guo, Y.; Huang, L.; Xue, Y.; Chen, J.; Yu, G.; Jiang, L.; Hu, W.; Liu, Y. Uniform Hexagonal Graphene Flakes and Films Grown on Liquid Copper Surface. *Proc. Natl. Acad. Sci. U.S.A.* **2012**, *109*, 7992–7996.
26. Wu, Y. A.; Fan, Y.; Speller, S.; Creeth, G. L.; Sadowski, J. T.; He, K.; Robertson, A. W.; Allen, C. S.; Warner, J. H. Large Single Crystals of Graphene on Melted Copper Using Chemical Vapor Deposition. *ACS Nano* **2012**, *6*, 5010–5017.
27. Novoselov, K. S.; Fal'ko, V. I.; Colombo, L.; Gellert, P. R.; Schwab, M. G.; Kim, K. A Roadmap for Graphene. *Nature* **2012**, *490*, 192–200.
28. Bonaccorso, F.; Sun, Z.; Hasan, T.; Ferrari, A. C. Graphene Photonics and Optoelectronics. *Nat. Photonics* **2010**, *4*, 611.
29. Wu, W.; Liu, Z.; Jauregui, L. A.; Yu, Q.; Pillai, R.; Cao, H.; Bao, J.; Chen, Y. P.; Pei, S. S. Wafer-Scale Synthesis of Graphene by Chemical Vapor Deposition and its Application in Hydrogen Sensing. *Sens. Actuator, B* **2010**, *150*, 296–300.
30. Lin, Y. M.; Valdes-Garcia, A.; Han, S.-J.; Farmer, D. B.; Meric, I.; Sun, Y.; Wu, Y.; Dimitrakopoulos, C.; Grill, A.; Avouris, P.; et al. Wafer-Scale Graphene Integrated Circuit. *Science* **2011**, *332*, 1294–1297.
31. Liu, Y.; Dobrinsky, A.; Yakobson, B. I. Graphene Edge from Armchair to Zigzag: The Origins of Nanotube Chirality? *Phys. Rev. Lett.* **2010**, *105*, 235502.
32. Papageorgiou, D.; Evangelakis, G. Multiple Excitations and Self-Diffusion Processes On and Near the Cu(110) Surface by Molecular Dynamics Simulations. *Surf. Sci.* **2000**, *461*, L543–L549.
33. Wood, J. D.; Schmucker, S. W.; Lyons, A. S.; Pop, E.; Lyding, J. W. Effects of Polycrystalline Cu Substrate on Graphene Growth by Chemical Vapor Deposition. *Nano Lett.* **2011**, *11*, 4547–4554.
34. Nie, S.; Wu, W.; Xing, S.; Yu, Q.; Bao, J.; Pei, S.; McCarty, K. F. Growth From Below: Bilayer Graphene on Copper by Chemical Vapor Deposition. *New J. Phys.* **2012**, *14*, 093028.
35. Artacho, E.; Sanchez-Portal, D.; Ordejon, P.; Garcia, A.; Soler, J. Linear-Scaling *Ab-Initio* Calculations for Large and Complex Systems. *Phys. Status Solidi B* **1999**, *215*, 809–817.
36. Junquera, J.; Paz, O.; Sanchez-Portal, D.; Artacho, E. Numerical Atomic Orbitals for Linear-Scaling Calculations. *Phys. Rev. B* **2001**, *64*, 235111.